Seismic response of sands in centrifuge tests

Mohammad H.T. Rayhani and M. Hesham El Naggar

Abstract: Seismic site response of sandy soils and seismic soil–structure interaction are investigated using an electro-hydraulic earthquake simulator mounted on a centrifuge container at an 80*g* field. The results of testing uniform and layered loose to medium-dense sand models subjected to 13 simulated earthquakes on the centrifuge are presented. The variation of shear modulus and damping ratio with shear strain amplitude and confining pressure was evaluated and their effects on site response were assessed. The evaluated shear modulus and damping ratio agreed reasonably with laboratory tests and empirical relationships. Site response analysis using the measured shear wave velocity and estimated modulus reduction and damping ratio as input parameters produced good agreement with the measured site response. The effect of soil–structure interaction for structures situated on dry sand is also investigated. These tests have revealed many important insights with regard to the characteristics of seismic site response and seismic soil–structure behaviour. The tests showed that the seismic response of soil deposits, input motions, and overall behaviour of the structure are affected by soil stratification. The results showed that the seismic kinematic soil–structure interaction is not very significant for structures situated on loose sand.

Key words: seismic response, soil–structure interaction, centrifuge modeling, amplification.

Résumé : On étudie la réponse sismique d'un site de sols sableux et l'interaction sismique sol–structure au moyen d'un simulateur de séisme électrohydraulique monté sur un godet de centrifuge dans un champ de 80*g*. On présente les résultats d'essais sur des modèles de sable uniforme et en couches molles à médium denses soumis à 13 séismes simulés dans le centrifuge. On a évalué la variation du module de cisaillement et du rapport d'amortissement avec l'amplitude de la déformation en cisaillement et la pression de confinement, et on a estimé leurs effets sur la réaction du site. Le module de cisaillement et le rapport d'amortissement évalués concordaient raisonnablement bien avec les essais de laboratoire et les relations empiriques. L'analyse de la réaction du site au moyen de la vélocité de l'onde de cisaillement mesurée et de la réduction du module et du rapport d'amortissement estimés comme paramètres d'intrant a produit une bonne concordance avec la mesure de la réaction du site. On a aussi étudié l'effet de l'interaction sol–structure pour les structures situées sur le sable sec. Ces essais ont révélé plusieurs éclaircissements importants en rapport avec les caractéristiques de la réponse sismique du site et le comportement sismique sol–structure. Les essais ont montré que la réponse sismique des dépôts de sol, les mouvements des intrants et le comportement global de la structure sont affectés par la stratification du sol. Les résultats montrent que l'interaction sol-structure cinématique sismique n'est pas tellement significatif pour les structures situées sur le sable meuble.

Mots-clés : réaction sismique, interaction sol–structure, modélisation par centrifuge, amplification.

[Traduit par la Rédaction]

Introduction

During earthquakes, seismic waves are generated in the bedrock and propagate through the soil layers and cause damage to structures resting on the surface. Recent destructive earthquakes, including the 1985 Michoacan earthquake in Mexico, the 1989 Loma Prieta and 1994 Northridge earthquakes in California, and the 1997 Kobe earthquake in Japan have revealed the role of local site conditions in modifying the characteristics of strong motion data. The nature of the subsoil influences the free-field seismic response by amplifying the seismic excitation originating at the bedrock as it travels through the overlying soil. Local site effects can cause significantly different amounts of structural damage in the same general area. Often, softer geologic conditions cause larger amplification of the seismic wave. The understanding of local site effects on strong ground motion is of particular importance for the mitigation of earthquake disasters, and for future earthquake-resistant design. It is also necessary to evaluate the response and the deformation of the ground against strong motion for vital structures, such as highrise buildings.

Dynamic centrifuge modeling is an effective tool for studying the effects of earthquakes on soil and soil–structure systems. Constitutive models and numerical procedures can be clearly tested using centrifuge model tests. Also, numerical models and procedures can be calibrated and improved or modified for phenomena that may not have been adequately accounted for in a model. A significant number of centrifuge experiments using ground motion simulation have been performed. Most of these experiments were carried out on liquefaction of saturated sand and pore-pressure investigation in sands and embankments (e.g., Adalier and Elgamal 2001; Elgamal et al. 2005). Shear modulus and damping

Received 24 October 2006. Accepted 15 October 2007. Published on the NRC Research Press Web site at cgj.nrc.ca on 22 April 2008.

M.H.T. Rayhani.[1] Department of Civil Engineering, Queen's University, Kingston, ON K7M 7H5,Canada.
M.H. El Naggar. Department of Civil and Environmental Engineering, University of Western Ontario, London, ON N6A 5B9, Canada.

[1]Corresponding author (e-mail: mrayhani@ce.queensu.ca).

degradation curves for saturated and dry sands, as well as soft clay, were investigated by Brennan et al. (2005) using dynamic centrifuge data. They concluded that evaluation of the stiffness of these materials was more reliable than evaluation of their damping ratio. Stevens et al. (2001) performed centrifuge tests on dense Nevada sand to evaluate numerical site response procedures under a wide range of earthquake intensities and sinusoidal sweeps. A new procedure was applied to produce shear modulus and shear strain time histories using a moving window technique. However, limited research is available regarding the soil amplification in loose and, especially, layered soil.

Scope of research

The objective of the research described in this paper is to investigate the seismic response of loose to medium-dense sand under dynamic base excitation. The research included subjecting soil profiles of uniform and layered loose to medium-dense sand to seismic loading using the 5 m radius Centre for Cold Ocean Resources Engineering (C-CORE) geotechnical centrifuge. The amplification of the earthquake motion through different soil profiles while considering different excitation levels and frequency contents was analyzed with special emphasis on seismic soil–structure interaction.

Soil properties

The soil used in the tests was well-graded, medium angular dried Al white silica sand with an effective diameter D_{50} = 0.288 mm and particle sizes in the range of 0.075–0.59 mm. Table 1 summarizes the sand properties. A standard density test of the sand showed that it has a maximum unit weight of 15.88 kN/m^3 and a minimum unit weight of 12.70 kN/m^3. The relative density of the loose and medium-dense soil samples was about 35%–70%, respectively.

Table 1. Properites of test sand.

Effective diameter, D_1	0.162
D_{50} (mm)	0.289
Uniformity coefficient,	2.063
Curvature coefficient,	1.052
Maximum void ratio, e_{max}	1.046
Minimum void ratio, e_{min}	0.637
Minimum density (Mg/m^3)	1.295
Maximum density (Mg/m^3)	1.619
Friction angle, ϕ (°)	35
Initial relative density (%)	
Model RS-05	35
Model RS-06	35, 70

Centrifuge modeling

Centrifuge models were prepared and tested on the large beam centrifuge at 80*g* in the C-CORE centrifuge centre. The soil models were prepared in a container with inner dimensions of 0.73 m in length, 0.3 m in width, and 0.57 m in height. An electrohydraulic earthquake simulator mounted on the centrifuge was used to apply a one-dimensional (1D) prescribed base input motion. Tests were performed on uniform loose dry sand and layered medium-dense sand models.

Figure 1 shows the view of the soil models with the containment structure and instrumentation (dimensions in prototype scale). A rigid structure model was slightly embedded in the soil. The centrifuge models were instrumented to measure free-field and foundation accelerations, free field displacements, and local deformations on basement walls and foundation slab. The models were subjected to earthquake excitations with different accelerations.

Model preparation

High-quality specimens are essential for obtaining reliable test results of site response and soil–structure interaction (SSI) analysis. Sand samples for centrifuge tests can be prepared by tamping, vibration, or raining (pluviation). Sand beds were prepared using a raining technique to provide a relatively uniform specimen with the desired relative density. The sand was poured into the package through a hopper system. The void ratio of the sand was controlled by the height and flow rate of sand pouring. The falling height was kept constant to obtain consistent relative density for the sand samples in the container. During the raining procedure, samples of 10^{-4} m^3 were taken to monitor the relative density and uniformity of the sand obtained in the centrifuge package. The accelerometers were inserted into the soil at the predetermined locations. When the required height of sand was achieved, the surface of the sand was leveled by a modified vacuum cleaner. The uniformity of the soil samples was checked by evaluating the relative density of the soil at the beginning and end of the flight, and cone penetration tests (CPTs) were conducted upon the completion of testing in flight. The raining technique implemented in this study produced reasonably uniform and consistent soil samples (Rayhani 2007).

Two models (packages) were prepared for centrifuge testing. The total thickness of sand in each model was approximately 0.375 m, simulating 30 m in prototype scale. The first model, RS-05, included loose uniform sand at an initial relative density, D_r = 35%. The second model, RS-06, contained 10 m of loose sand with D_r = 35% overlying 20 m of medium-dense sand with D_r = 70%. In each package, a rigid structure model was embedded in the soil to simulate the behaviour of soil–structure interaction for earthquake motion. At 80*g*, the resulting bearing stress underneath the structure was 95 kPa. This arrangement provided a reasonable simulation for the behaviour of a rectangular 10-storey building.

Two types of instrumentation were used in all models: (*i*) accelerometers for measuring acceleration, and (*ii*) linear variable differential transformers (LVDTs) for measuring displacements. The accelerometers were placed within the soil bed at predetermined positions. Accelerometers were also placed on the structure top and walls and LVDTs were positioned on the structure model and on top of the soil surface to measure vertical displacements and soil surface settlements.

Model testing

When model preparation was completed, the package was carefully moved onto the centrifuge arm using a forklift. All instrumentation was then connected to the signal box, and the model surface profile was measured on the centrifuge arm. The centrifuge rotational speed was gradually increased

Fig. 1. Centrifuge models configuration in prototype scale. LVDT, linear variable differential transformers; A_c, accelerometer; z, depth.

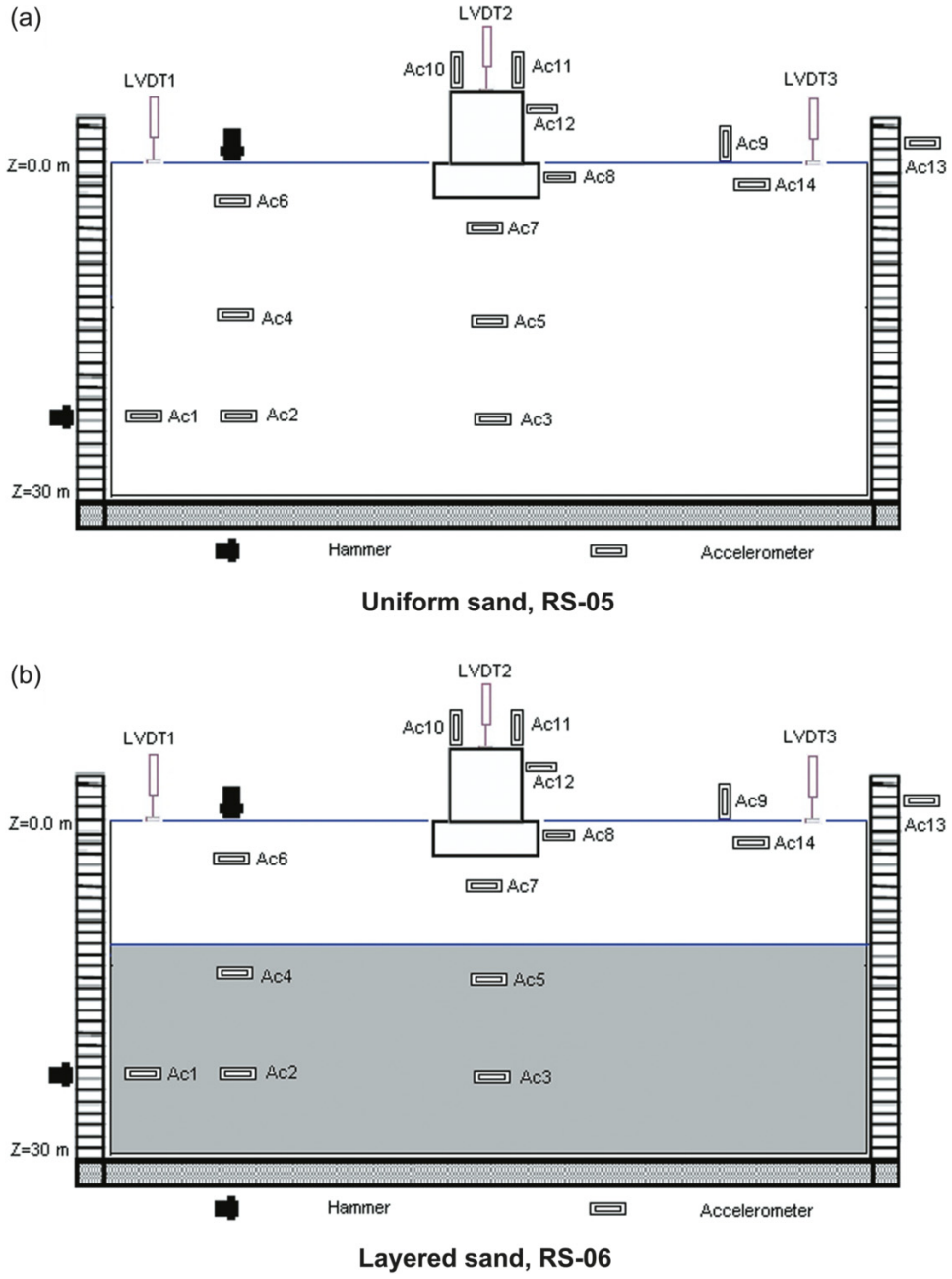

from stationary (swing-up) until a gravity level of 80g was reached. Displacement measurements were taken continuously to measure soil settlement and ensure that the instruments were functioning correctly. The P-wave velocity measurements were conducted at each 10g in the container. The CPTs were carried out to determine the soil shear strength profile at 80g. The earthquake input motions of the 2A2475 West Canada event, developed for Mitchell Island in the Fraser Delta (Seid-Karbasi 2003), and the actual recordings of the Port Island downhole array –79 m record northeast component from the Kobe earthquake were fired at 80g. The earthquake loading ranged from small-amplitude shakes to large events (Table 2). All data were collected using a highspeed data acquisition system.

Shear strength profile

Cone penetration tests were performed in-flight using a miniature penetrometer to determine the shear strength profile of the soil at 80g. Phillips and Valsangkar (1987) reported results of CPT tests in sand performed at penetration rates of 2–4 mm/s with no noticeable difference in results. The test was carried out by pushing the penetrometer into the soil model container at a penetration rate of 3 mm/s.

Figure 2a shows the CPT tip resistance profile at 80g for both models. The tip resistance, q_c, varied from 5–14 MPa for model RS-05 and from 5–10 MPa for the upper loose layer and 25–32 MPa for the lower layer in model RS-06. Based on the empirical correlation of $q_c - \tan\phi'$ established by Robertson and Campanella (1983) for CPT tests in nor-

Table 2. Shear wave velocity of soil in centrifuge container.

Centrifuge gravity (g)	Confining pressure, σ_c (kPa)	V_s (m/s)	
		RS-05	RS-06
10	35	125	135
20	70	131	143
30	106	139	151
40	142	143	172
50	177	156	192
60	213	161	208
70	248	167	227
80	283	172	238

mally consolidated sands, the internal friction was about 36°–38° for the loose sand and 40°–41° for the medium-dense sand, where ϕ' is the effective friction angle.

Shear wave velocity measurement

The shear wave velocity in the centrifuge model was evaluated using the hammer test for each centrifuge gravity level at 20 m depth. The test involves generating and propagating compression waves that can be detected by the arrays of accelerometers in the soil model. The test procedure consisted of striking the steel base plate of the model soil container with a sledgehammer. Differential travel times were computed by identifying the compression wave arrivals at each accelerometer, and the compression wave velocity, V_p, was then computed from the accelerometer positions. Travel times were estimated using the first strong peak interpretation method. The measurements of V_p were obtained at progressively increasing g levels of 10g to 80g. The shear wave velocity (V_s) was estimated based on V_p and the soil Poisson's ratio, ν (assumed to be 0.3 in this study based on resonant column test results Khan (2007) on a similar sand):

$$[1] \qquad (V_p/V_s) = [(1-\nu)/(0.5-\nu)]^{0.5}$$

The shear wave velocity measured from the hammer test was obtained for the lower soil layer only. Therefore, the shear wave velocity profile was estimated using established relations (Andrus et al. 2005) between CPT tip resistance and shear wave velocity for sandy soils. The relationship was developed based on V_s and CPT tip resistance for sands considering the age of the sample, i.e.,

$$[2] \qquad V_s = 77.4(q_c)^{0.178}\mathrm{ASF}$$

where q_c is normalized cone tip resistance, and ASF is the age scaling factor.

Earthquake shaking events

Each model was subjected to six earthquake-like shaking events. The input excitations were scaled versions of an artificial western Canada earthquake, developed for Mitchell Island in the Fraser Delta (Seid-Karbasi 2003) and the actual recordings of the Port Island downhole array –79 m record northeast component from the Kobe earthquake. Details of shaking events are shown in Table 3. The earthquake motions were applied using the electrohydraulic simulator described by Coulter and Phillips (2003). Input motions varied between 5.6g and 63g, at target frequencies from 40 to 200 Hz (modeling prototype earthquakes between 0.07g and 0.79g).

Test results

The test results are discussed with respect to seismic soil properties and accelerations and settlements recorded at various depths and locations.

Shear wave velocity

The soil shear wave velocity (V_s) is provided in Table 3 for a range of confining pressure estimated by hammer tests at lower level of the centrifuge container. The equivalent confining pressure for each gravity level was estimated assuming coefficient of earth pressure at rest K_0 = 0.5 and octahedral stress. Table 2 shows that the shear wave velocity increased as the confining pressure increased. The measured shear wave velocity varied between 125 and 172 m/s in RS-05 (loose sand) and between 135 and 238 m/s in model RS-06 (medium-dense sand). The average shear wave velocity of the 30 m soil profile was about 149 and 179 m/s for models RS-05 and RS-06, respectively.

The shear wave velocity of only the lower soil layer was measured from the hammer test. Therefore, the shear wave velocity profile along the soil model was estimated from the correlation with CPT measurements for both models (Fig. 2*b*). The estimated shear wave velocity was slightly less than that evaluated from the *P*-wave measurements.

Settlement

The settlement of the soil surface was measured using LVDTs attached to the model racks and extended downward to pads placed at the soil surface. To measure structural settlement, an LVDT was used on top of the structure. Figure 3 depicts the swing-up settlement curves from 1g to 80g for the free field and structure in prototype scale. The maximum structure settlement was about 55 mm for RS-05 and 25 mm for RS-06, and the free-field settlements were 5–10 mm less. This shows that the soil densified as the model spun up from 1g to 80g, especially in loose sand (RS-05). The settlement was also measured at the end of each earthquake excitation. The maximum seismic settlement varied from 1 mm for event KL (peak acceleration a_{max} = 0.07g) to 95 mm for KH (a_{max} = 0.49g), which shows that the soil continued to densify as the test progressed with higher strength excitation. The change in D_r was calculated from the measured settlement as the gravity field reached 80g, assuming 1D settlement. The relative density at 80g was estimated to be about 37.5% and 72% for loose and medium-dense sand, respectively.

Accelerations

The measured peak horizontal accelerations at the free field and beneath the structure at different depths are presented in Table 4 for both models. The acceleration time history A3 (close to the bottom of the models) was similar in shape and magnitude to the input motion. Accelerometers A6 and A7 recorded the surface acceleration at the free field and beneath the structure, respectively. It is noted from Table 4 that accelerations generally increased from the base to

Fig. 2. (*a*) Shear strength from CPT test, (*b*) V_s profile for both soil models.

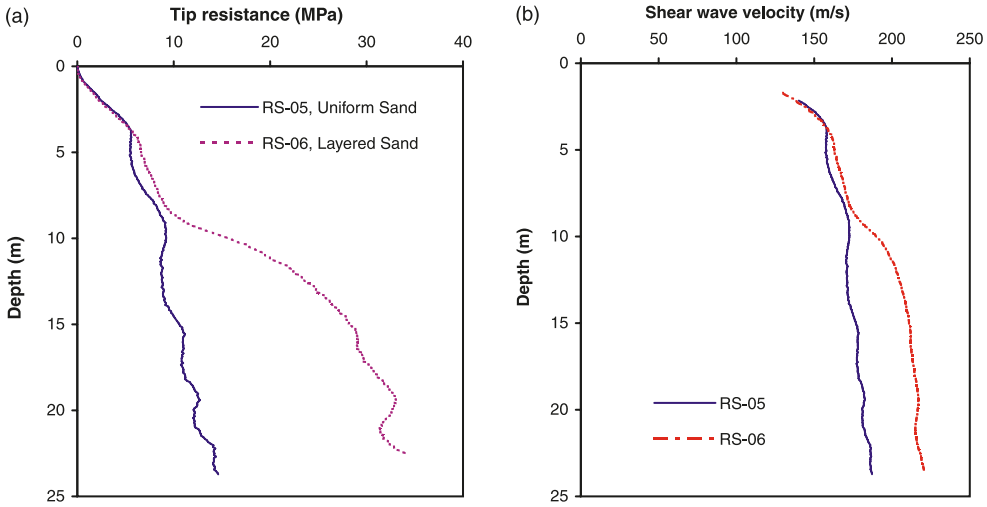

Table 3. Earthquake input motion in centrifuge tests.

	Prototype		Centrifuge (scale 1:80)	
Event	Peak acceleration (*g*)	Frequency at peak (Hz)	Peak acceleration (*g*)	Frequency at peak (Hz)
WCL	0.1	0.93	8	7.5
WCM	0.17	0.93	14	7.5
WCH	0.39	0.93	31	7.5
KL	0.07	2.19	5.6	175
KM	0.22	2.19	17.6	175
KH	0.49	2.19	39	175
KVH	0.79	2.19	63	175

Note: WCL, western Canada low; WCM, western Canada medium; WCH, western Canada high; KL, Kobe low; KM, Kobe medium; KH, Kobe high; KVH, Kobe very high.

the surface in low and medium shaking events and slightly attenuated for high shaking events. The accelerations of the free field and beneath the structure were similar and were less than the peak structure acceleration (A12).

Analysis and discussion

Variation in relative density

The soil experienced cyclic shear stresses during earthquake events. In the case of loose sand, cyclic shear stress would densify the soil. The relative density changes were estimated using the LVDT measurements at the end of each shaking event and assuming 1D settlement; the results are shown in Fig. 4. The relative density increased substantially as the test progressed with higher strength excitation. The change in relative density was not significant for weak shaking events (KL and WCL), but D_r increased from 37.5% to 39.5% for stronger events (e.g., $a_{max} = 0.49g$). These results are in good agreement with those of Siddharthan et al. (2004) for Nevada sand. The increase in relative density would affect the frictional resistance and soil stiffness. Therefore, there would be an increase in bearing capacity of the structure.

Evaluation of shear stress and shear strain histories

The shear stress and shear strain histories were evaluated using the procedure proposed by Zeghal et al. (1995). Shear stress and shear strain response at a particular depth can be obtained using the recorded lateral accelerations, assuming 1D vertically propagating shear waves. The shear stress at any depth was estimated by integrating the equation of an idealized 1D shear beam as

$$[3] \qquad \tau(z,t) = \int_0^z \rho\, \ddot{u}\, \mathrm{d}z$$

where z is the depth coordinate; t is time; τ is the horizontal shear stress, $\ddot{u}$ is the horizontal acceleration, and ρ is the density. Linear interpolation between accelerations was employed to evaluate the shear stress at each level. To calculate the shear strain, displacement records were obtained through double integration of the corresponding recorded acceleration histories. Knowing the spacing between the accelerometers, the shear strain histories were then evaluated from the displacement data.

Accuracy of shear stress and shear strain estimates is a function of accelerometer configuration, data processing, and employed analysis technique (Zeghal et al. 1995). Displacement histories from integration of accelerations often include base-line drifts. Bandpass filters were employed between 0.03 and 25 Hz to eliminate noise in the high-frequency range and drifts in the low-frequency range. The filter bandwidths were selected wide enough to preserve the real shear stress and shear strain characteristics of the soil model. Considering the close spacing of accelerometers and simplicity of analysis, first order linear interpolation between accelerations and second-order interpolation between displacements were employed to evaluate the shear stress and shear strain, respectively. The estimated data are sensitive to filtration. As recommended by Brennan et al. (2005), the filtration has to be performed prior to the second integration for displacement as well.

The estimated seismic shear stress and shear strain histories are related by the soil shear stiffness characteristics at each accelerometer level (Zeghal et al. 1995). The shear stress – strain hystereses at different depths in model RS-05 during different shaking events are shown in Fig. 5.

The WCL event provided a low-strain soil response, and

Fig. 3. Settlement curve from 1*g* to 80*g* for both soil profiles.

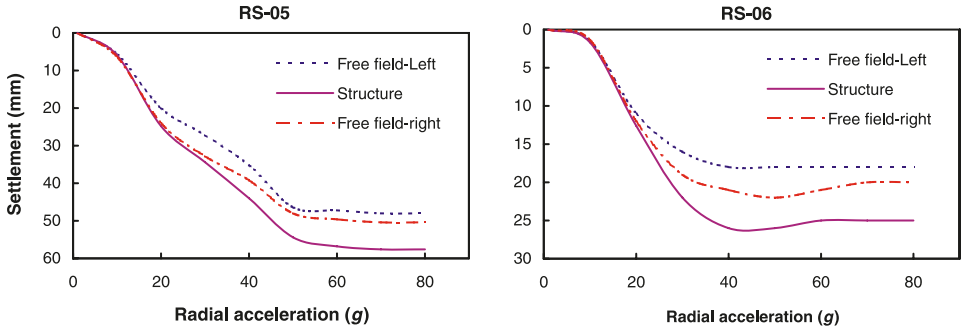

Table 4. Peak acceleration at free field, structure, and beneath the structure.

Model event	Base acceleration, *(g)*	RS-05, uniform sand					RS-06, layered sand				
		A3	A6	A7	A8	A12	A3	A6	A7	A8	A12
WCL	0.10	0.11	0.12	0.12	0.12	0.15	0.10	0.11	0.11	0.11	0.16
WCM	0.17	0.17	0.23	0.24	0.24	0.26	0.18	0.20	0.19	0.21	0.29
WCH	0.39	0.38	0.36	0.37	0.37	0.41	0.42	0.37	0.39	0.39	0.46
KL	0.07	0.08	0.10	0.10	0.10	0.13	0.08	0.09	0.09	0.10	0.13
KM	0.22	0.20	0.25	0.26	0.26	0.28	0.21	0.27	0.27	0.29	0.35
KH	0.49	0.48	0.51	0.49	0.49	0.56	0.50	0.51	0.53	0.53	0.66
KVH	0.79	—	—	—	—	—	0.75	0.81	0.79	0.78	0.84

Fig. 4. Relative density variation in both sand models for all shaking events.

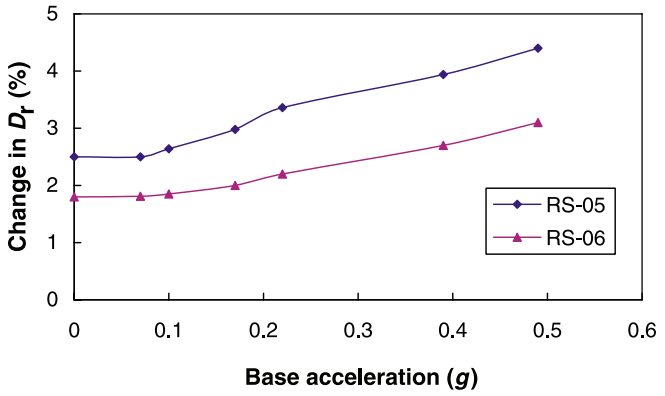

the slope of the hysteresis loop increased with an increase in the depth of the accelerometer, indicating the effect of confining pressure on soil shear stiffness. The shear strain level increased with the application of stronger shaking events to the soil model (WCM and WCH), and the soil shear stiffness, manifested by the slope of the hysteresis loop, decreased with an increase in the the strain amplitude. The shear stress – strain area, and thus the soil damping, increased with an increase in strain amplitude and decreased with an increase in depth. These behaviours are in good agreement with reported results in the literature (Seed and Idriss 1970; Hardin and Drnevich 1972).

Shear modulus and damping ratio

The soil equivalent shear modulus and damping ratio were evaluated from the stress–strain cycles of the WCL, WCM, and WCH earthquake shakings at different depths as a function of shear strain amplitude. These shaking events produced shear strains ranging from about 0.1% to 1.0%. The equivalent shear modulus was estimated using the secant slope of the representative shear stress–strain loop (Kramer 1996) for each shaking event at 3, 12, and 20 m depth, i.e.

$$[4] \qquad G = \frac{\tau(\gamma_m)}{\gamma_m}$$

where γ_m is the maximum shear strain amplitude, and τ is the associated shear stress. To compare measured shear moduli with standard degradation curves, the moduli were normalized by the small-strain shear modulus, G_{max}, evaluated from the hammer test measurements. The estimated value of G_{max} was about 34 MPa at 3 m depth, 42 MPa at 12 m depth, and 45 MPa at 20 m depth. The damping ratio was calculated from selected stress–strain loops at 3, 12, and 20 m using the area of the actual shear stress – strain loop, A_{loop} (Kramer 1996):

$$[5] \qquad \xi = \frac{A_{loop}}{2\pi\gamma^2}$$

Shear modulus

Shear modulus values were derived from three accelerometers aligned vertically up the free-field model (A2, A4, and A6) and were normalized by G_{max}. The shear modulus degradation curves for accelerometers A6 (3 m depth), A4 (12 m depth), and A2 (20 m depth) are shown in Fig. 6*a* and are compared with the curves generated from the empirical relationships given by Hardin and Drnevich (1972) and Seed and Idriss (1970) for dry fine sands. A best fit through results obtained from appropriate resonant column data at 300 kPa confining pressure (Rayhani 2007) is also plotted in Fig. 6*a* for comparison.

Fig. 5. Shear stress – shear strain hystereses at different depths in model RS-05.

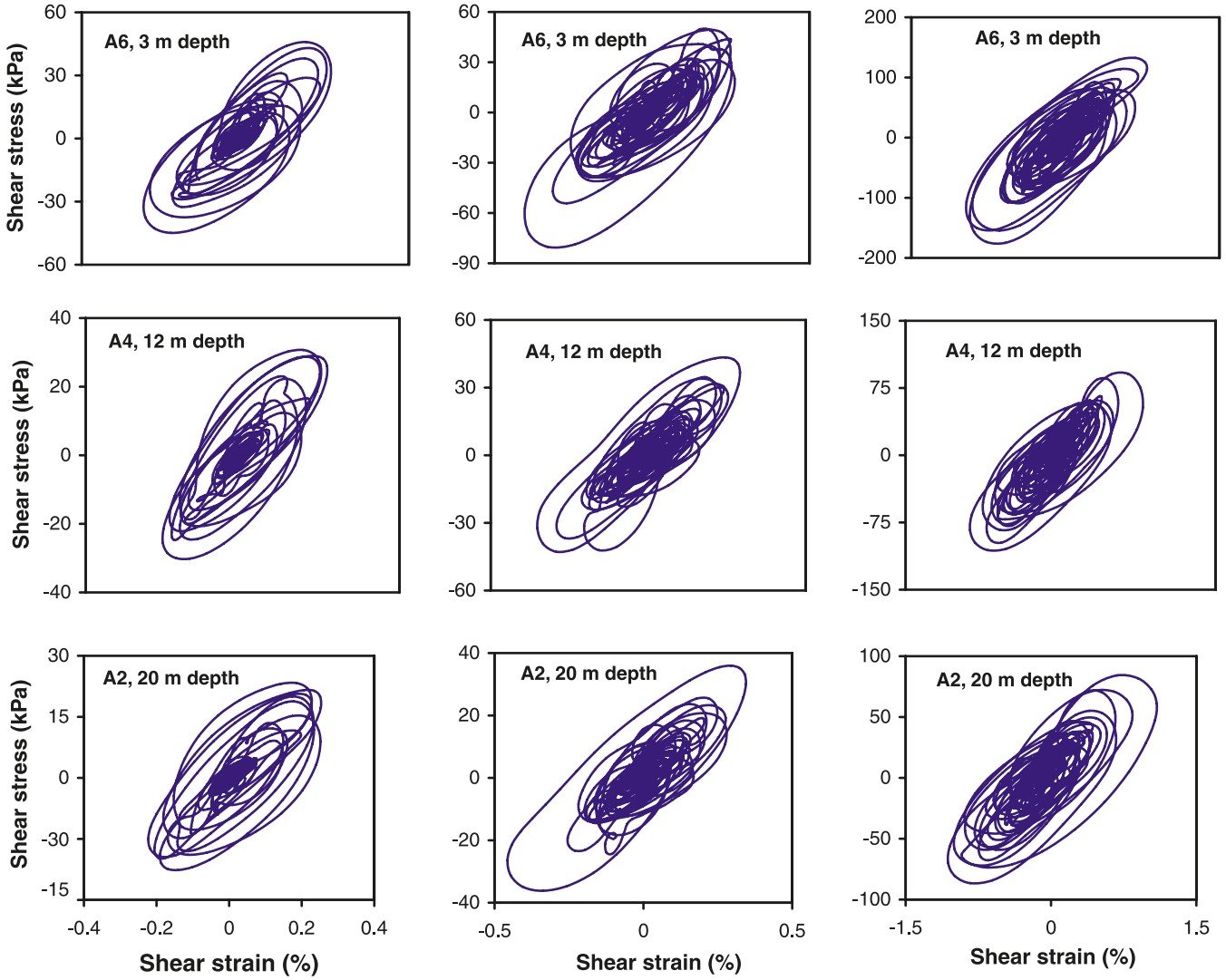

The shear modulus data appear to be close to the resonant column results and the design curve proposed by Hardin and Drenvich (1972) at all strain levels, especially in the lower depths (confining pressures). However, the centrifuge data seem to be higher than those obtained from the empirical relations and element test results. This behaviour may be attributed to densification of loose sand during higher magnitude events. Figure 5*a* also shows that the shear modulus increased as the confining pressure (depth) increased.

Damping ratio

Figure 6*b* presents the damping ratios evaluated from the centrifuge test results, a best fit line of the damping ratio of the resonant column tests and the design curve proposed by Hardin and Drnevich (1972) and Seed and Idriss (1970). As expected, the damping ratios decreased with an increase in depth (or confining pressure) and increased with an increase in shear strain amplitude. The comparison of the centrifuge data with empirical relations and element tests shows a reasonable agreement with the empirical curves, especially the relation proposed by Hardin and Drnevich. The damping ratio at smaller strain ranges is close to that obtained from resonant column tests. However, the damping ratio at shear strain magnitudes larger than 0.5% is slightly higher than the corresponding Hardin and Drnevich and Seed and Idriss empirical curves. This scatter in damping could be due to densification of loose sand and stronger soil particle contact during strong earthquake excitation. Frictional energy loss in the soil skeleton is increased as the soil particles gain contact with each other (Brennan et al. 2005; Zeghal et al. 1995). Such scatter in damping was also observed in investigations of damping such as that of Brennan et al. (2005). The damping ratio is in reasonable agreement with the empirical curves of Hardin and Drnevich and Seed and Idriss and the resonant column results for shear strains smaller than 0.5%.

Comparison of calculated and recorded responses

Site response analyses were performed for each shaking event using equivalent linear analysis in the program QUAKE/W (GEO-SLOPE International Ltd. 2004). The centrifuge shear wave velocity measurements and estimated shear modulus and damping ratios were used as input to these analyses. Since V_s data were obtained for the lower

Fig. 6. Shear modulus degradation and damping ratio in model RS-05.

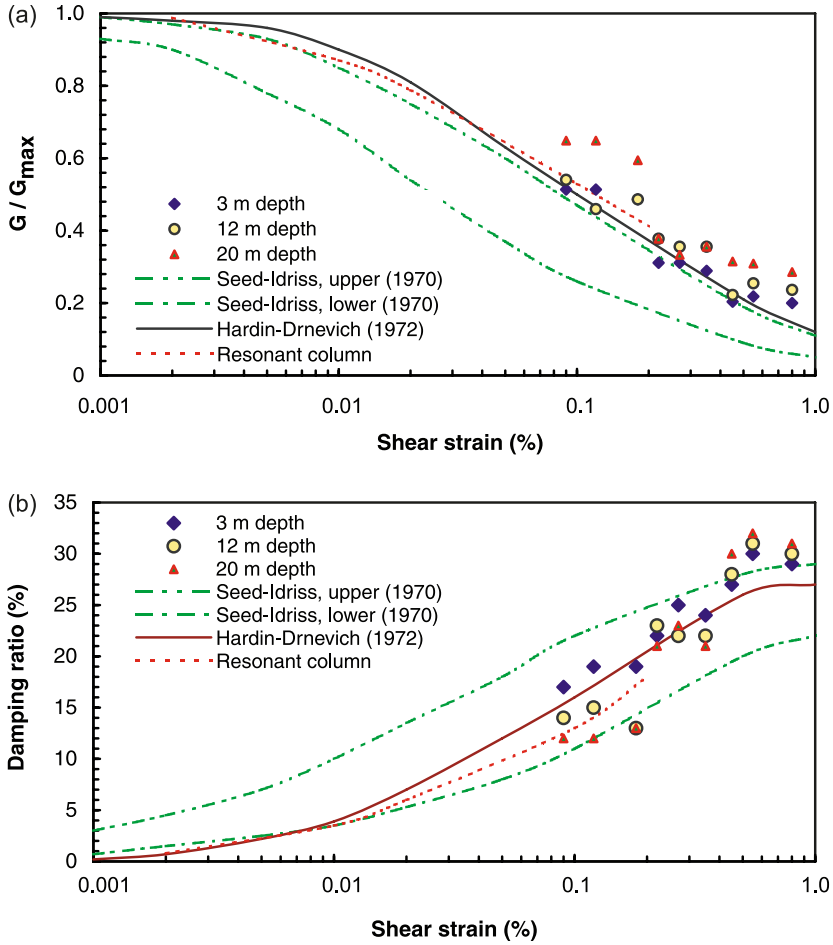

soil layer, the shear wave velocity profile estimated from the CPT test was used for response analysis. The modulus reduction relationship was taken as the upper range and the damping ratio was taken as the lower range proposed by Seed and Idriss (1970), since they were close to the measured data. The recorded time history at the base of the centrifuge container was used as the base input motion of the soil profile in the analyses. Calculated and recorded acceleration time histories and the corresponding response spectra in model RS-05 for the WCM earthquake motion at different depths are compared in Fig. 7, which shows that the calculated and recorded response are in good agreement at all depths. The strain level in numerical analysis was found to be slightly lower than that from the model tests. For example, the strain level in event WCM at the free field is about 0.042%, whereas in QUAKE/W analysis it was about 0.035%.

Amplification of motion

Three accelerometers were placed along a vertical plane far from the structure to study the free-field acceleration amplification, and a similar setup was used to evaluate the amplification beneath the structure (see Fig. 1). Figure 8*a* depicts the acceleration amplifications (i.e., peak recorded accelerations normalized by the corresponding base peak acceleration) in both uniform and layered soil profiles at different depths for all shaking events. It is noted from Fig. 8*a* that the acceleration was amplified for weak excitations in both models. The amplification factor was as high as 1.35 and 1.28 near the surface in event KL (a_{max} = 0.07*g*) for uniform and layered soil profiles, respectively. In the case of a strong shaking event with a_{max} = 0.49*g*, a slight attenuation occurred (i.e., de-amplification of 0.96) in uniform loose soil but there was no amplification for the layered soil. This behaviour is attributed to soil nonlinearity during the strong shaking.

Figure 8*b* compares the surface (free-field) motion amplification with that beneath the structure for all shaking events and shows that they are almost the same for both models, indicating that the kinematic soil–structure interaction is not very significant in the loose sand, especially beneath the structure. This behaviour is similar to the results of Ghosh and Madabhushi (2003) on silica sand with a relative density of 45%. As the strength of the earthquake was increased (with peak accelerations 0.39*g* and 0.49*g*) the amplification factor was significantly reduced due to the nonlinear soil behaviour.

Spectral analysis

Spectral analysis was used to characterize the frequency content of the strong input motion imposed on the structure and establish the predominant frequency of the earthquake loading. The response spectra of the models for event WCM (a_{max} = 0.17*g*) at the free field and beneath the struc-

Fig. 7. Acceleration time histories and response spectra (5% damping) in model RS-05 for event WCM (a_{max} = 0.17g).

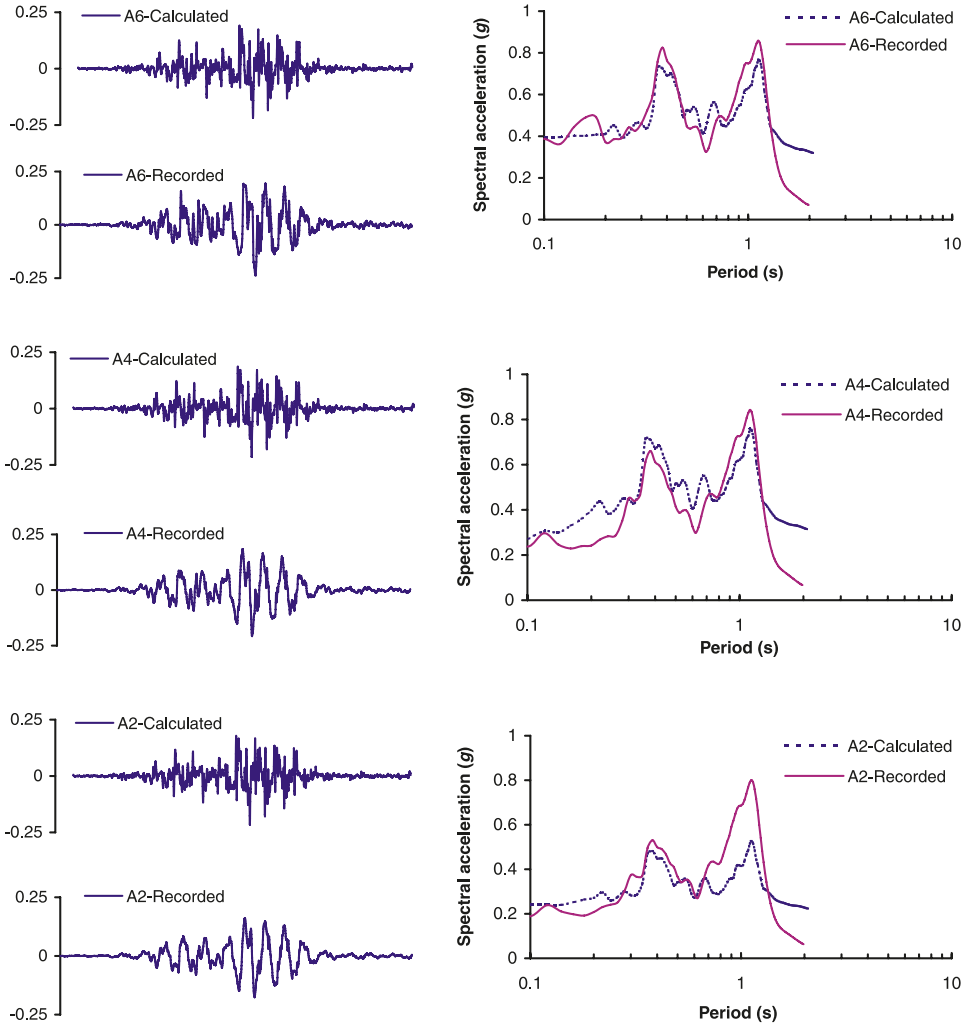

ture are shown in Fig. 9. It is noted from the figure that the acceleration response was amplified for low periods, especially in the range 0.3–0.6 s, which reflects the local site effects on the input motion. The peak surface spectral acceleration was about 0.83g for RS-05 and 0.75g for RS-06. The motion of the soil beneath the structure was almost the same as free-field motion in terms of amplitude and frequency content.

The relationship between the vibration periods of the model structure and predominant period of the supporting soil influences the seismic response of structures. The stiffness and natural period of the model structure were estimated for both soil profiles and are shown in Table 5. As can be seen from Table 5 and Fig. 9, amplification beneath the structure (accelerometer A7) has occurred close to the natural period of the model structure, whereas amplifications for other accelerations occurred close to the natural period of the site (0.3–0.6 s). The horizontal stiffness of the system decreased (i.e., natural period increased) with an increase in the earthquake excitation due to the shear modulus degradation during the earthquake excitation. The natural period for the layered soil profile was slightly less than that for the uniform loose sand, as the average shear modulus for the layered model was higher.

Figure 10 shows the ratio of response spectra (RRS) curves or transfer functions, obtained by normalizing the acceleration response near the ground surface by those of the base. The maximum values of RRS for event WCM were about 2.5 and 3.3 for RS-05 and 2.3 and 2.7 for RS-06 at the free-field soil and beneath the structure, respectively. The maximum RRS for soil beneath the structure was slightly higher than the free-field acceleration, which shows slight kinematic soil–structure interaction in both soil profiles. The natural frequency of the soil deposit was estimated from its thickness and shear wave velocity and was found to be 0.26 and 0.21 s for RS-05 and RS-06, respectively. This provides a useful indication of the frequency of vibration at which the most significant amplification can be expected (Kramer 1996). It is noted from Fig. 10 that the amplifications occurred in the vicinity of the soil deposit natural period.

The transfer function of the site response (RRS) was used to assess the ground motion amplification and seismic hazard associated with different period earthquakes. Figure 11a shows the variation of the peak RRS frequency with shaking amplitude for the free field and beneath the structure. The peak frequency for RS-05 was higher than that for RS-06 for both the free field and beneath the structure, especially

Fig. 8. (*a*) Variation of amplification factor with depth. (*b*) Amplification factor for both free field and beneath the structure. *a* and *A*, peak base acceleration.

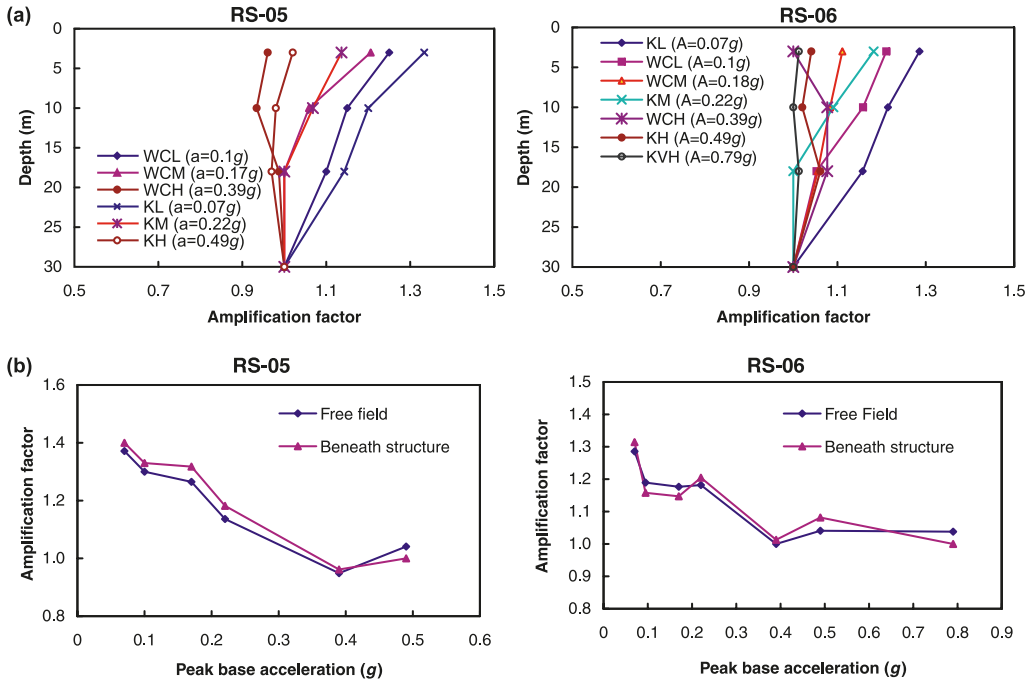

Fig. 9. Response spectra of the models with peak base acceleration of 0.17*g*.

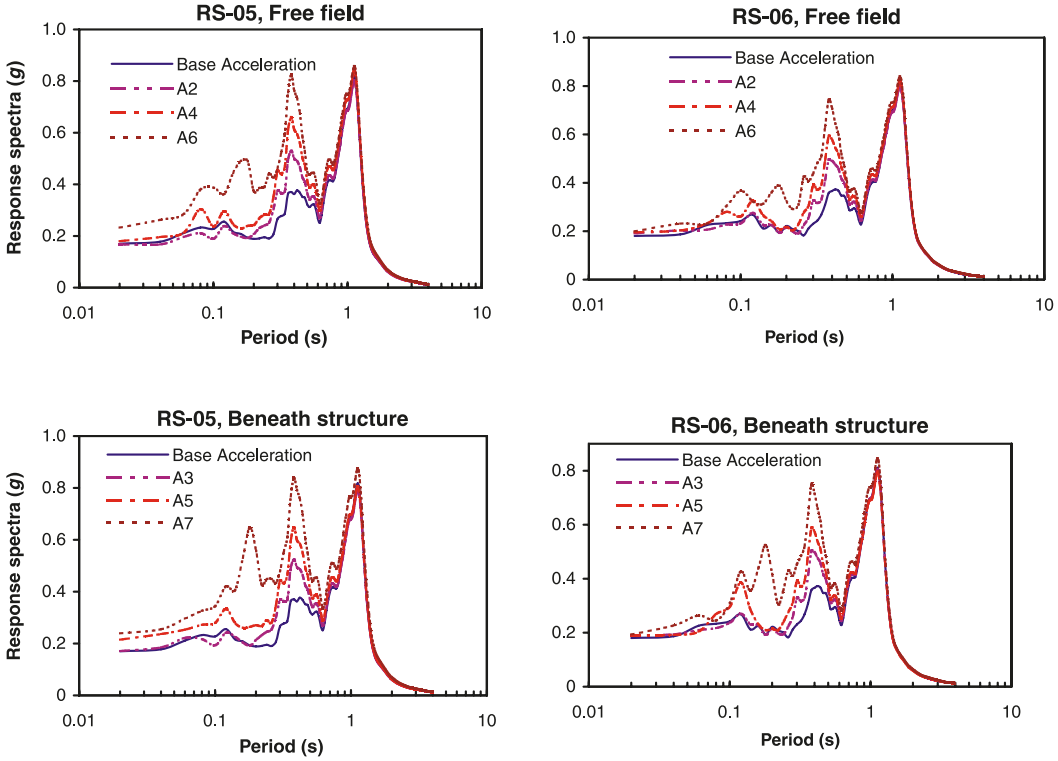

in weak shakings. The frequency at which the maximum RRS occurred decreased with an increase in the earthquake intensity. These results are in good agreement with experimental findings for soft soils in a centrifuge container by Yu and Lee (2002). The peak frequency for RS-05 decreased from 6.2 Hz for a low shaking event to 2.5 Hz for a stronger event, and that for RS-06 decreased from 4.3 Hz for a low shaking event to 2.6 Hz for a strong shaking event. The peak frequencies in the free field and beneath the structures are almost the same for both models.

The variation of maximum RRS with base shaking amplitudes is shown in Fig. 11*b*. The maximum RRS decreased in

Table 5. Stiffness and natural period of the model structure.

	Stiffness, K_u (N/m × 10^8)		Natural period (sec)	
Event	Model RS-05	Model RS-06	Model RS-05	Model RS-06
WCL	3.48	5.12	0.18	0.14
WCM	2.55	3.76	0.21	0.17
WCH	1.58	2.43	0.26	0.21

both soil models as the earthquake intensity increased. The maximum RRS for the weak shaking event ($a_{max} = 0.1g$) in RS-05 was about 3.2 and 3.4 for free field and beneath the structure, respectively; and about 2.6 at both locations for the strong event ($a_{max} = 0.49g$). For RS-06, RRS was 2.3 and 2.4 for free field and beneath the structure, respectively for the weak shaking event and 1.9 and 1.8 for the strong event ($a_{max} = 0.79g$). These results show that RRS increased with an increase in the thickness of loose sand, similar to the observations of Yu and Lee (2002) for thick soft ground in weak earthquakes. The reduction in maximum RRS for stronger shakings is attributed to the soil's nonlinear response and its limited ability to transfer stresses to upper layers as the strength of the soil was reached. The progressive degradation of soil stiffness due to the cyclic shear strain amplitude could soften the soil (Ghosh and Madabhushi 2003). Thus, the system may undergo resonance at lower shakings while the higher shakings are being attenuated. Furthermore, at high strain levels the soil material damping increases as the earthquake amplitude increases, further reducing the response.

Structural behaviour

The structural response was recorded by accelerometers A8 embedded in soil adjacent to the structure and A12 attached to the building wall. Vertical accelerometers were attached to the top of the structure on both sides to measure possible rocking behaviour.

The spectral accelerations of A8 and A14 (free field) are compared in Fig. 12 to evaluate the interference of the structure with horizontal ground motion. The response spectra near the structure were slightly higher than those at the free field at low periods, but almost the same level in higher periods. This means that there was no significant alteration of the ground motion due to the presence of the structure. The difference in response of A8 and A14 in the layered profile was slightly higher than that of the uniform soil for the same shaking event. This may be attributed to the concentration of nonlinearity within the top soil layer (adjacent to the structure) in the layered soil profile. The ratio of accelerations at A7 and A8 to those at A14 are compared in Fig. 13 to evaluate the structure effects on ground motion behaviour. It is noted that these ratios are close to unity in RS-05, indicating an insignificant effect of soil–structure interaction (kinematic) on the ground motion. For RS-06, the ground motion ratio beside the structure was slightly higher than that beneath it in weak shakings and slightly less in stronger shakings. This was attributed to the nonlinearity concentrated in the loose sand.

The inertial soil–structure interaction was evaluated by comparing readings from accelerometer A12 (attached to the structure wall) with accelerometers A14 and A8. It is noted that A12 experienced higher acceleration (10%–20%) than both A14 and A8 for both models due to inertial SSI, and the peak structural acceleration in RS-06 was slightly higher than that in RS-05.

Vertical accelerometers A10 and A11 were attached to the top of the structure, one on each side, to capture possible rocking behaviour. Figure 14 shows the rocking response during all shaking events, which was calculated as the difference between the displacements of both sides of the structure normalized by the distance. A negligible rocking angle was observed for both models, suggesting the structure experienced negligible rocking.

Absolute displacements of different points were obtained by integrating the measured accelerations, and relative movement of different points could be obtained by subtracting their respective absolute displacements. The relative lateral movement of the structure (and its sliding) during an earthquake shaking was estimated by subtracting displacement of A7 from displacement of A8. The maximum relative lateral movement of the structure has been plotted in Fig. 15*a* for all shaking events. It can be noted that the movement of the structure was negligible for low shaking events, but increased with the level of shaking. For example, it was about 0.4 and 0.5 mm (prototype scale) for uniform and layered profiles for event WCM and 1.8 and 2.9 mm for event KH.

Permanent settlement of the structure was evaluated from LVDT measurements at the end of each earthquake loading and is shown in Fig. 15*b*. The maximum structural settlement was 90 mm in RS-05 and 55 mm in RS-06. This clearly demonstrates that the soil densified as the earthquake strength increased, especially in the case of loose sand.

Summary and conclusions

Centrifuge tests of uniform and layered loose dry sand profiles with a model structure were subjected to several earthquake-like shaking events to study the seismic site response of loose soil and seismic soil–structure interaction.

The evaluated shear modulus and damping ratio from centrifuge data varied with an increase in depth: the shear modulus increased and the damping ratio decreased. The identified shear modulus reduction seemed to be relatively close to that from the empirical relations, in comparison with other published data in the literature. However, the modulus values were slightly higher than those from the empirical relations, especially at shear strain magnitude larger than 0.5%. The damping ratio was in reasonable agreement with the empirical curves. However, there is a slight scatter in the data at shear strain larger than 0.5%.

The recorded accelerations indicated that the peak accelerations at the surface were amplified for weak earthquakes and slightly attenuated for strong earthquakes. This is attributed to nonlinear soil behaviour and an increase in soil material damping for high strain levels. Also, higher amplification ratios were recorded for earthquakes with lower frequency content (i.e., greater distance from earthquake source and higher magnitude). The peak accelerations close to the soil surface were almost similar for both the free field and beneath the structure, indicating insignificant kinematic soil–structure.

Fig. 10. Ratio of surface response spectra (RRS) to base response spectra, $a_{max} = 0.17g$.

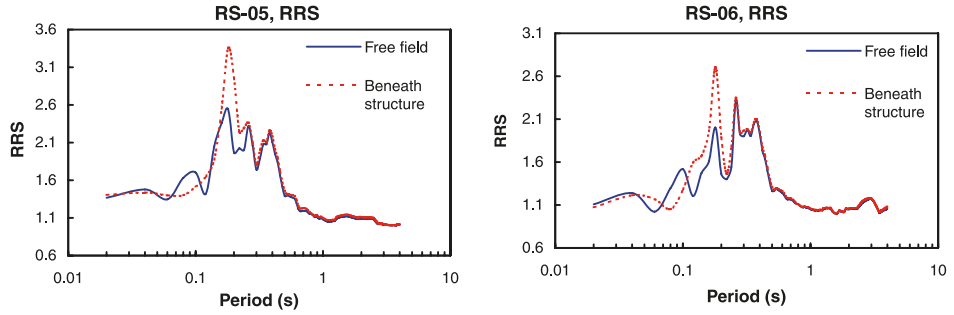

Fig. 11. Variation of (*a*) frequency at peak RRS, and (*b*) maximum RRS with base shaking amplitude.

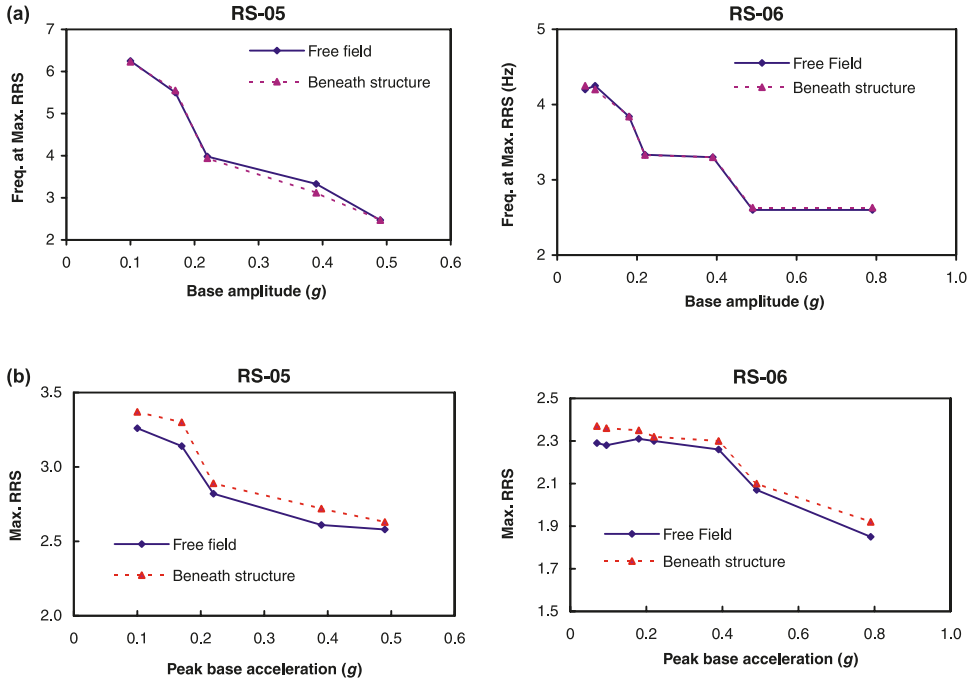

Fig. 12. Horizontal variation of response spectra beside (A8) and far from (A14) the structure.

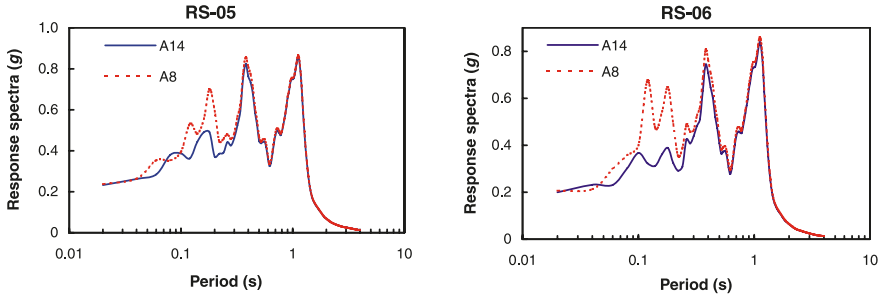

The soil densified considerably during the model swing-up, thus the actual sand relative density was different from the initial values. The densification was increased as the test progressed with higher excitation strengths. It is expected that the soil strength and stiffness would be higher after the earthquake event, and that the capacity of the foundation would increase accordingly.

The motion of soil beneath the structure was almost the same as the free-field motion in terms of amplitude and frequency content. The peak frequency in uniform loose sand was higher than that of the layered profile, especially in weak shakings. The frequency at which the maximum ration of the response spectra (RRS) occurred decreased with an increase in the earthquake intensity. This is attributed to a decrease in the soil shear modulus and increase in its damping ratio. The maximum RRS trend was almost similar in the free field and beneath the structure in both soil models, but the maximum RRS of the layered soil profile was less than that of uniform sand.

Negligible structural rocking and lateral movement were

Fig. 13. Ground input motion ratio.

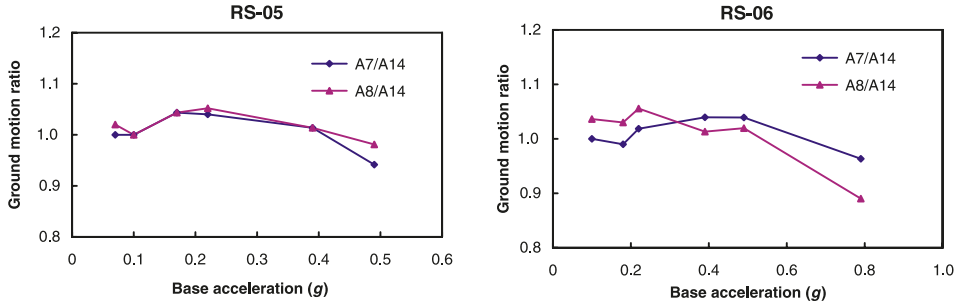

Fig. 14. Structural rocking during shaking event WCM.

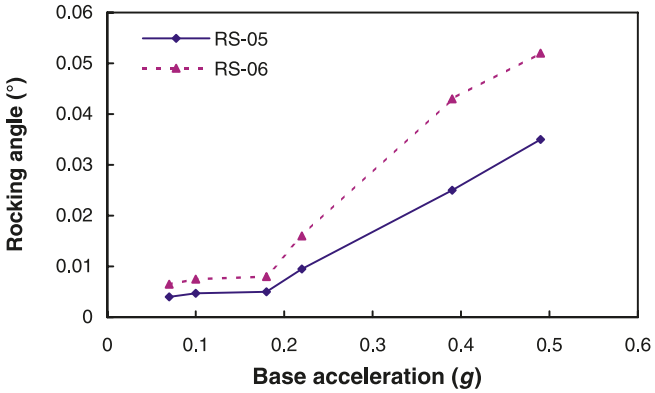

Fig. 15. (*a*) Relative lateral movement, and (*b*) permanent settlement of the structure for all shaking events.

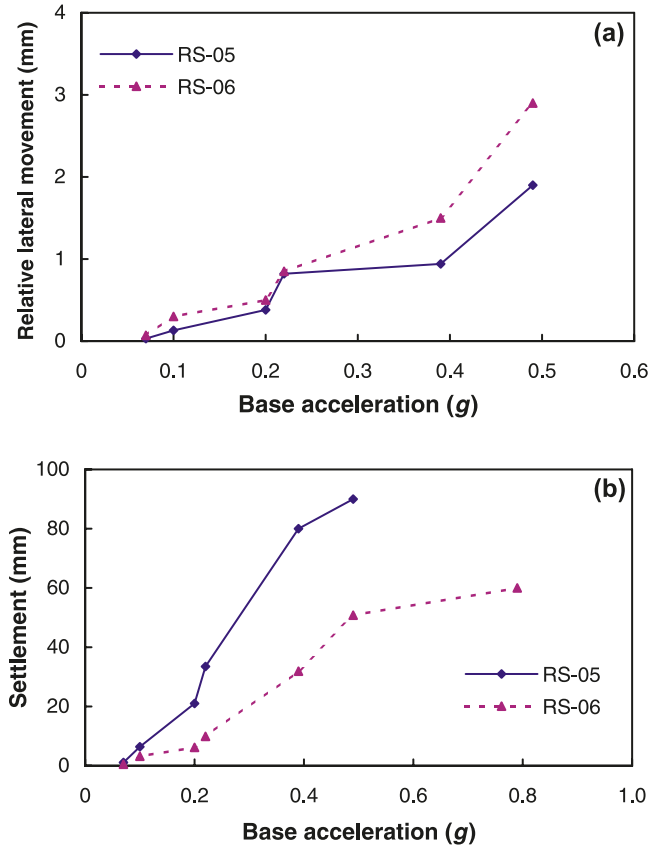

observed during all shaking events for both soil profiles. Permanent settlement of the structure in loose sand was greater than that in the layered soil profile, as expected, and the maximum settlement was within tolerable foundation settlement.

Acknowledgements

The authors would like to thank Dr. Ryan Phillips, director of the physical modeling department at C-CORE, for his guidance and support during the centrifuge testing phase of this research and Gerry, Susan, Karl, Don Cameron, and Derry for their assistance in the centrifuge tests. Their help is gratefully acknowledged.

References

Adalier, K., and Elgamal, A.W. 2001. Seismic response of dense and loose sand columns. *In* Proceedings of 4th International Conference on Recent Advances in Geotechnical Earthquake Engineeringand Soil Dynamics, San Diego, Calif., 26–31 March 2001. *Edited by* S. Prakash, University of Missouri-Rolla, Rolla, Mo. Paper 4.19.

Andrus, R.D., Pitatheepan, P., and Juang, C.H. 2005. Shear wave velocity – penetration resistance correlations for ground shaking and liquefaction hazard assessment. Clemson University, Clemson, S.C. Report 01HQGR0007.

Brennan, A.J., Thusyanthan, N.I., and Madabhushi, S.P.J. 2005. Evaluation of shear modulus and damping in dynamic centrifuge tests. Journal of Geotechnical and Geoenvironmental Engineering, ASCE, **131**(12): 1488–1497. doi:10.1061/(ASCE)1090-0241(2005)131:12(1488).

Coulter, S.E., and Phillips, R. 2003. Simulating submarine slope instability initiation using centrifuge model testing. *In* Proceedings of the 1st International Symposium on Submarine Mass Movements and Their Consequences, EGS–AGU–EUG Joint Assembly Meeting, Nice, France. Kluwer Academic Publishers, Dordrecht, the Netherlands. Paper ISSMM-062.

Elgamal, A., Yang, Z., Lai, T., Kutter, B.L., and Wilson, D.W. 2005. Dynamic response of saturated dense sand in laminated centrifuge container. Journal of Geotechnical and Geoenvironmental Engineering, ASCE, **131**(5): 598–609. doi:10.1061/(ASCE)1090-0241(2005)131:5(598).

GEO-SLOPE. 2004. QUAKE/W: computer program for seismic response analysis for horizontally layered soil deposits. GEO-SLOPE International, Calgary, Alta.

Ghosh, B., and Madabhushi, S.P.G. 2003. Effect of localized soil inhomogenity in modifying seismic soil structure interaction. *In* Proceedings of the ASCE 16th Engineering Mechanics Conference, Seattle, Wash., 16–18 July 2003, ASCE, New York. pp. 1–8.

Hardin, B.O., and Drnevich, V.P. 1972. Shear modulus and damp-

ing in soil: design equations and curves. Journal of the Soil Mechanics and Foundations Division, ASCE, **98**: 667–692.

Khan, Z. 2007. Dynamic characterization of soils: effects of frequency and loading amplitude. Ph.D. thesis, University of Western Ontario, London, Ont.

Kramer, S.L. 1996. Geotechnical earthquake engineering. Prentice Hall, Upper Saddle River, N.J.

Phillips, R., and Valsangkar, A.J. 1987. An experimental investigation of factors affecting penetration resistance in granular soils in centrifuge modeling. Cambridge University Engineering Department, Cambridge, UK. Technical Report CUED/D-Soils TR210.

Rayhani, M.H.T. 2007. Centrifuge modeling of seismic site response and soil–structure interaction. Ph.D. thesis, University of Western Ontario, London, Ont.

Robertson, P.K., and Campanella, R.G. 1983. Interpretation of cone penetration tests. I: Sand. Canadian Geotechnical Journal, **20**(4): 718–733. doi:10.1139/t83-078.

Seed, H.B., and Idriss, I.M. 1970. Soil moduli and damping factors for dynamic response analyses. Earthquake Engineering Research Center (EERC), University of California at Berkeley, Berkeley, Calif. Report EERC-70/10.

Seid-Karbasi, M. 2003. Input motion time histories for dynamic testing in the C-CORE centrifuge facilities. University of British Columbia, Vancouver, B.C. Report 2003/01.

Siddharthan, R.V., Ganeshwara, V., Kutter, B.L., El-Desouky, M., and Whitman, R.V. 2004. Seismic deformation of bar mat mechanically stabilized earth walls. 1: Centrifuge tests. Journal of Geotechnical and Geoenvironmental Engineering, ASCE, **130**(1): 14–25. doi:10.1061/(ASCE)1090-0241(2004)130:1(14).

Stevens, D., Kim, B., Wilson, D., Kutter, B., and Elgamal, A. 2001. Centrifuge model tests to identify dynamic properties of dense sand for site response calculations. *In* Proceedings of the 4th International Conference on Recent Advances in Geotechnical Earthquake Engineering and Soil Dynamics, San Diego, Calif., 26–31 March 2001. *Edited by* S. Prakash. University of Missouri-Rolla, Rolla, Mo. Paper 1.66, pp. 26–31.

Yu, Y., and Lee, F.H. 2002. Seismic response of soft ground. *In* Proceedings of the International Conference on Physical Modeling in Geotechnics (ICPMG'02), St. John's, Nfld., 10–12 July 2002. *Edited by* R. Phillips, P. Guo, and R. Popescu. Swets & Zeitinger, Lisse. pp. 519–524.

Zeghal, M., Elgamal, A.-W., Tang, H.T., and Stepp, J.C. 1995. Lotung downhole array. II: evaluation of soil nonlinear properties. Journal of Geotechnical Engineering, ASCE, **121**: 363–378. doi:10.1061/(ASCE)0733-9410(1995)121:4(363).